Mechanistic Aspects of the Covalent Flavoprotein Dimethylglycine Oxidase of *Arthrobacter globiformis* Studied by Stopped-Flow Spectrophotometry†

Jaswir Basran,‡ Nina Bhanji,‡ Amrik Basran,§ Daniel Nietlispach,|| Sharad Mistry,⊥ Rolandas Meskys,# and Nigel S. Scrutton*,‡

Department of Biochemistry, University of Leicester, University Road, Leicester LE1 7RH, U. K., Institute of Biotechnology, University of Cambridge, Tennis Court Road, Cambridge CB2 1QT, U. K., Department of Biochemistry, University of Cambridge, 80 Tennis Court Road, Cambridge CB2 1GA, U. K., Protein and Nucleic Acid Laboratory, University of Leicester, Centre for Mechanisms of Human Toxicity, Lancaster Road, Leicester LE1 9HN, U.K., and Laboratory of Microbiology and Biotechnology, Institute of Biochemistry, Mokslininku 12, Vilnius, Lithuania

Received January 7, 2002; Revised Manuscript Received February 19, 2002

ABSTRACT: Dimethylglycine oxidase (DMGO) is a covalent flavoenzyme from *Arthrobacter globiformis* that catalyzes the oxidative demethylation of dimethylglycine to yield sarcosine, formaldehyde, and hydrogen peroxide. Stopped-flow and steady-state kinetic studies have been used to study the reductive and oxidative half-reactions using dimethylglycine and O_2 as substrates. The reductive half-reaction is triphasic. The rate of the fast phase is dependent on substrate concentration, involves flavin reduction, and has a limiting rate constant of 244 s^{-1}. This phase also displays a kinetic isotope effect of 2.9. Completion of the first kinetic phase generates an intermediate with broad spectral signature between 350 and 500 nm, which is attributed to a reduced enzyme−iminium charge-transfer species, similar to the purple intermediate that accumulates in reactions of D-amino acid oxidase (DAAO) with alanine. The second phase (16 s^{-1}) is independent of substrate concentration and is attributed to iminium hydrolysis/deprotonation. The third phase (2 s^{-1}) is attributed to product release, the rate of which is less than the steady-state turnover rate (10.6 s^{-1}). Flavin oxidation of dithionite- and dimethylglycine-reduced enzyme by O_2 occurs in a single phase, and the rate shows a linear dependence on oxygen concentration, giving bimolecular rate constants of 342 and 201 mM^{-1} s^{-1}, respectively. Enzyme-monitored turnover experiments indicate that decay of the reduced enzyme−iminium intermediate is rate-limiting, consistent with rate constants determined from single turnover studies. A minimal kinetic mechanism is presented, which establishes a close relationship to the mechanism of action of DAAO. The covalent flavin in dimethylglycine oxidase is identified as an αN^1-histidyl^{48}-FAD, and equilibrium titration studies establish a single redox center that displays typical flavoprotein 'oxidase' characteristics.

Amine oxidation is widespread in biology, and a number of enzymes have evolved to catalyze these reactions. The wide distribution of these oxidative reactions reflects the multiple roles for amine compounds, for example, in cell growth, cancerogenesis, and differentiation, DNA binding, neurotransmission, and apoptosis (*1*−*5*). Amine oxidases and dehydrogenases responsible for these reactions can be grouped broadly into the flavoprotein and quinoprotein families. In yeasts and bacteria, these enzymes facilitate growth on a number of primary, secondary, and tertiary amine compounds. Owing to the relative ease of purifying the bacterial and yeast enzymes, they have become important model systems for investigating the mechanisms of amine oxidation from structural (*6*−*10*) and kinetic/spectroscopic [e.g., (*11*−*15*)] viewpoints.

The mechanisms of amine oxidation catalyzed by the quinoprotein amine oxidases are reasonably well understood and occur through the formation of enzyme−substrate covalent adducts with topaquinone or tryptophan tryptophylquinone redox centers (*16*, *17*). In some cases, the quinoprotein amine oxidases have become important models for the study of hydrogen transfer by quantum tunneling mechanisms (*18*−*20*). The oxidation of amines by three flavoproteins has also been shown to occur by the quantum transfer of hydrogen (*14*, *21*, *22*), but the chemical mechanism of C−H bond cleavage remains equivocal (*23*−*26*). A number of studies now indicate that the oxidation of amines by flavoenzymes probably occurs through the formation of a covalent adduct by the nucleophilic attack of the substrate nitrogen at the flavin C4a position (*7*, *11*, *22*, *27*). Abstraction of hydrogen from substrate by the flavin N5 atom then facilitates cleavage of the substrate C−H bond. A similar mechanism has been proposed for the oxidation of substrates by DAAO[1] (*28*).

† This work was funded by grants from the BBSRC and the Lister Institute of Preventive Medicine. N.S.S. is a Lister Institute Research Professor.

* Correspondence should be addressed to this author at the Department of Biochemistry, University of Leicester, University Rd., Leicester LE1 7RH, U.K. Tel: +44 116 223 1337; Fax: +44 116 252 3369; E-mail nss4@le.ac.uk.

‡ Department of Biochemistry, University of Leicester.

§ Institute of Biotechnology, University of Cambridge.

|| Department of Biochemistry, University of Cambridge.

⊥ University of Leicester, Centre for Mechanisms of Human Toxicity.

Laboratory of Microbiology and Biotechnology, Institute of Biochemistry.

10.1021/bi025519h CCC: $22.00
Published on Web 03/14/2002

In developing further our interest in the mechanism of amine oxidases, we have cloned the gene (*dmg*) encoding dimethylglycine oxidase (DMGO), a novel covalent flavoprotein oxidase from *Arthrobacter globiformis*, and expressed and purified the protein (*29*). At the sequence level, DMGO is related to eukaryotic dimethylglycine dehydrogenase (*30*) and sarcosine dehydrogenase (*31*), and contains nucleotide-binding, flavinylation, and folate-binding motifs. DMGO catalyzes the oxidative demethylation of dimethylglycine in the reaction:

$$(CH_3)_2NCH_2COOH + O_2 + H_2O \rightarrow (CH_3)NHCH_2COOH + HCHO + H_2O_2$$

The reaction is functionally similar to that catalyzed by the monomeric and heterotetrameric sarcosine oxidases [MSOX (*6*) and TSOX (*32*), respectively]. However, at the primary structure level, DMGO shows very little sequence identity with MSOX and TSOX, suggesting major structural differences between DMGO and the sarcosine oxidases. In this paper, we report detailed stopped-flow kinetic studies of flavin reduction and oxidation in DMGO by dimethylglycine and dioxygen, respectively. We also report on the location of the covalent link between enzyme and flavin in DMGO, and a series of equilibrium spectroscopic studies of the enzyme in the presence of ligands, salts, and artificial and physiological reductants. Our studies establish the kinetic mechanism of DMGO and provide spectroscopic evidence suggesting the formation of a reduced flavin-iminium charge-transfer intermediate in the reductive half-reaction, similar to the 'purple' intermediate identified in reactions with DAAO (*33*−*35*), tyramine oxidase (*36*), and L-phenylalanine oxidase (*37*). We show that decay of the enzyme−iminium charge-transfer intermediate is rate-limiting in steady-state reactions catalyzed by DMGO.

EXPERIMENTAL PROCEDURES

Materials, Enzyme Purification, and Determination of Concentration. Recombinant DMGO was purified from *E. coli* strain JM109 transformed with plasmid pEH1 as described (*29*). The enzyme concentration was calculated using a molar extinction coefficient for the oxidized enzyme of $\epsilon_{444} = 12\,700\ M^{-1}\ cm^{-1}$ (calculated from absorption measurements of native and guanidine hydrochloride unfolded enzyme).

Molecular Weight Determination. High-resolution gel filtration chromatography of DMGO was performed using a Superdex 200 10/30 HR column on a Pharmacia FPLC system at 4 °C. The column was equilibrated with 50 mM sodium phosphate buffer, pH 7.5, containing 100 mM potassium chloride (buffer A) and calibrated using low and high molecular weight gel filtration calibration kits (Pharmacia) following the manufacturer's protocols. A calibration curve was constructed from a plot of log molecular weight of the native protein against K_{av}. DMGO (25 μg) was applied to the column and eluted with buffer A at a linear flow rate of 0.25 mL/min; the A_{280} of the eluant was monitored during the course of the experiment. Experiments were repeated in the presence of 200 and 400 mM KCl.

Isolation and Sequencing of Flavinylated Peptide. DMGO (3 mg) contained in 50 mM NH_4HCO_3 buffer, pH 7.8, was added to a solution containing 50 mM Tris-HCl, pH 8.0, 5 mM 2-mercaptoethanol, 5.6 M urea and the protein denatured by heating the sample at 95 °C for 25 min. The urea concentration was reduced to < 1 M by the addition of 50 mM NH_4HCO_3 buffer, pH 7.8, and trypsin was added such that the protease:protein ratio was 1:100. The sample was incubated at 37 °C in the dark for 24 h. Peptides produced from the trypsin-cleavage reaction were separated on a reverse-phase column (VYDAC catalog #208TP51) fitted with a guard column (VYDAC catalog #208GD51) using an HPLC system (Agilent model 1100) linked to a photodiode array detector. Solvents used were 0.1% trifluoroacetic acid (solvent A) and 0.1% trifluoroacetic acid in 80% acetonitrile (solvent B). Flow rate was 0.06 mL/min using the following gradient: 1% solvent B (0−10 min), 1−30% solvent B (10−12 min), 30−100% solvent B (12−90 min). Elution of peptides was monitored at 215 and 442 nm (flavin). Fractions with typical flavin absorbance spectra around 450 nm were collected and subjected to N-terminal sequence analysis on an Applied Biosystems model 476A protein sequencer. The isolated peptides were first covalently attached by the C-terminal carboxylic acid group to Sequelon-AA membrane (Millipore).

Identification of the Flavin by Nuclear Magnetic Resonance Spectroscopy. DMGO (42 mg) was solubilized in 4 M urea and 50 mM Tris-HCl, pH 7.5 (2 mL), and boiled for 10 min. After cooling to room temperature, 0.3% (w/w) trypsin was added, and the sample was incubated at 37 °C for 16 h. The digested protein was then passed through a Centricon-10 filtration unit to retain the trypsin and any undigested DMGO. The filtrate was concentrated using a Centricon-3 (3 kDa) filtration unit until the volume had been reduced to 300 μL. ^{31}P NMR experiments were recorded with proton decoupling at 25 °C using a Bruker DRX 500 spectrometer. Sample conditions were 100 mM Tris-HCl, pH 7.5, and 10% D_2O. The sample concentrations were 50 mM for FAD and FMN and 0.35 mM for trypsinised DMGO. Spectrum acquisition times were 2 min for the flavin samples and 12 h for DMGO. Free induction decays were apodized with 10 Hz line-broadening. All measured chemical shift values are reported relative to an external standard (85% phosphoric acid).

Preparation of Anaerobic Samples. Buffers were made anaerobic by bubbling argon gas through solutions for ~2 h. Solutions were then placed in an anaerobic glovebox (Belle Technology) overnight to remove any residual traces of oxygen. Samples of DMGO were made anaerobic by passing them through a small gel filtration (Bio-Rad 10 DG) column housed in the glovebox, which had been preequilibrated with anaerobic buffer. Solutions of dithionite and substrates were made by adding the appropriate solid to anaerobic buffer.

Circular Dichroism Spectroscopy. Circular dichroism spectroscopy was performed using a Jasco J-715 spectropolarimeter with 1 mm (far-UV measurements) and 10 mm (near-UV measurements) path lengths at 20 °C. Spectra were collected (over a wavelength range of either 190−260 or 250−500 nm) with a scan rate of 20 nm/min. Typically, 10 scans were recorded and averaged; no smoothing algorithms

[1] Abbreviations: DMGO, dimethylglycine oxidase; MSOX, monomeric sarcosine oxidase; TSOX, heterotetrameric sarcosine oxidase; PHBH, *p*-hydroxybenzoate hydroxylase; TMADH, trimethylamine dehydrogenase; DAAO, D-amino acid oxidase.

were employed. Protein sample concentrations were 1 mg/mL (near-UV measurements) and 0.2 mg/mL (far-UV measurements).

Steady-State Kinetic Assays. DMGO activity was measured by monitoring hydrogen peroxide formation using a horseradish peroxidase-coupled assay (*29*). Steady-state kinetic measurements were carried out using a Hewlett-Packard 8452A single beam diode array spectrometer with a 1 cm light path. Reactions were performed at 25 °C in 10 mM sodium pyrophosphate buffer, pH 8.5, containing 100 mM KCl, 0.05% *o*-dianisidine, 40 IU of horseradish peroxidase, and a fixed concentration of DMGO. The reaction was initiated by the addition of dimethylglycine, and initial rates were calculated from the absorbance increase at 430 nm (ϵ_{430} = 10 800 M^{-1} cm^{-1}). One unit of activity is defined as the amount of enzyme that catalyzes the production of 1 μmol of oxidized dye (1 μmol of H_2O_2 produced) per minute. Apparent K_m and k_{cat} values were determined by varying the concentration of protiated or deuterated dimethylglycine and fitting the data to the Michaelis−Menten equation using the Grafit software package (*38*).

Steady-state measurements were also performed using the enzyme-monitored turnover method as described by Gibson et al. for reactions catalyzed by glucose oxidase (*39*). Reactions were performed in an Applied Photophysics SX18-MV reaction analyzer. Solution conditions are described under Results. Data analysis was essentially as described elsewhere (*39*).

Stopped-Flow Kinetic Experiments. Stopped-flow experiments of reductive and oxidative half-reactions were performed using an Applied Photophysics SX.17 MV stopped-flow spectrophotometer. Reaction cell protein concentration was 4 μM (reductive half-reaction) or 5 μM (oxidative half-reaction) for single wavelength experiments and 20 μM for photodiode array experiments, and reactions were performed under anaerobic conditions. For this purpose, the sample-handling unit of the stopped-flow instrument was contained within a Belle Technology glovebox. All buffers were made oxygen-free by evacuation and extensive bubbling with argon before use. Buffers were then placed in the glovebox overnight before use. Unless otherwise stated, measurements were carried out at 25 °C in 10 mM sodium pyrophosphate buffer, pH 8.5.

Stopped-flow, multiple-wavelength absorption studies were carried out using a photodiode array detector and X-SCAN software (Applied Photophysics Ltd.). Spectral deconvolution was performed by global analysis and numerical integration methods using PROKIN software (Applied Photophysics Ltd.). In single wavelength studies, flavin reduction by substrate was observed at 444 nm. Transients were triphasic and were fitted using the standard triple exponential expression (eq 1):

$$A_{444} = C_1 e^{-k_{obs1}t} + C_2 e^{-k_{obs2}t} + C_3 e^{-k_{obs3}t} + b \quad (1)$$

where k_{obs1}, k_{obs2}, and k_{obs3} are the observed rate constants for the fast, intermediate, and slow phases respectively, C_1, C_2, and C_3 are the relative amplitude values for the three phases, and b is an offset value to account for a nonzero baseline. In studies of the oxidative half-reaction, enzyme was reduced anaerobically by titration with dithionite or dimethylglycine and rapidly mixed with buffer containing a known concentration of dioxygen. Oxidative transients were monophasic and analyzed using a standard single-exponential expression.

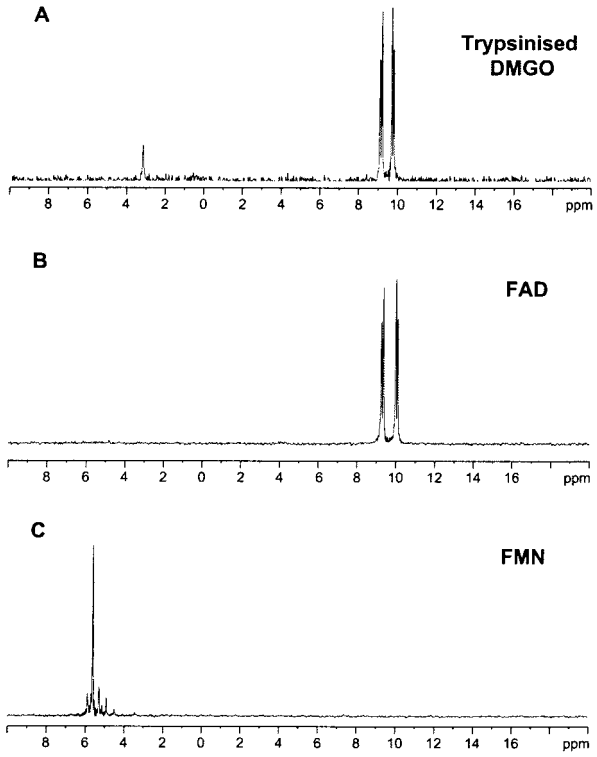

FIGURE 1: ^{31}P NMR spectra of trypsin-digested recombinant DMGO. Spectrum A, a sample of DMGO (0.35 mM) treated with trypsin as described under Experimental Procedures; spectrum B, FAD (50 mM); spectrum C, FMN (50 mM). Spectra recorded at 25 °C. Chemical shifts reported are relative to phosphoric acid.

RESULTS

Location of the Covalent Bond Linking the Flavin Cofactor to DMGO. The location of the flavin cofactor−DMGO bond was established by sequencing a flavinylated peptide isolated from a tryptic digest of DMGO, and by comparison of the sequence with the known sequence of the enzyme (*29*). Based on fluorescence properties, we demonstrated previously that the covalent flavin in DMGO is an αN^1-histidyl-flavin, although the site of attachment in the protein was not determined. In this paper, we have isolated a flavinylated peptide (identified by its absorbance at 442 nm) during HPLC purification of a tryptic digest of purified DMGO. Automated Edman degradation of this peptide identified the following sequence: GWNNITVLDQGPLNMPGGSTS*APGLVFQTNP, which corresponds to residues 27−58 in the sequence of DMGO (*29*). The asterisk indicates the position of His-48 in the peptide sequence, which corresponds to the lack of recognizable signal during automated Edman degradation. Residue His-48 in DMGO aligns with histidine residues in both rat and human dimethylglycine dehydrogenase and sarcosine dehydrogenase, which are known to be the sites of covalent attachment of flavin in these enzymes (*29*). ^{31}P NMR studies of a tryptic digest of the enzyme revealed the presence of two peaks with chemical shifts that are consistent with the presence of covalent FAD (Figure 1). The native molecular mass of DMGO is 210 ± 10 kDa, as determined by analytical

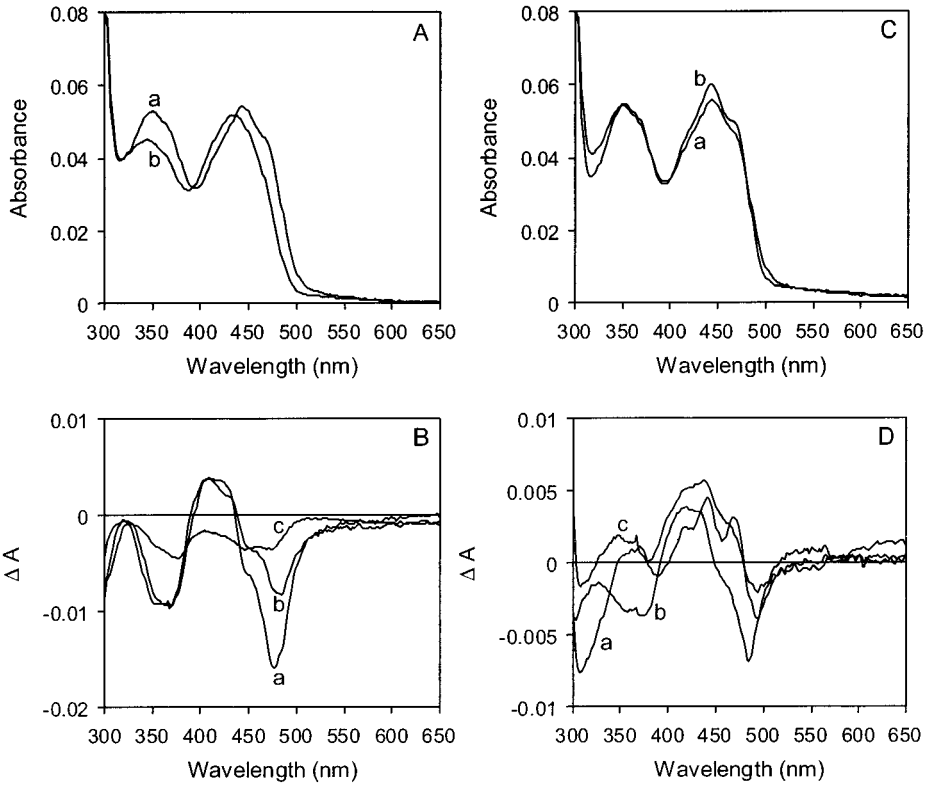

FIGURE 2: Spectra of DMGO in the presence and absence of salts. Panel A, spectrum of DMGO contained in 10 mM potassium phosphate buffer, pH 7.5, in the absence (spectrum a) and presence (spectrum b) of 200 mM KCl. Panel B, difference spectrum of DMGO (spectrum in the presence of salt minus spectrum in the absence of salt) for different halide salts of potassium (200 mM). Difference spectrum a, KCl; difference spectrum b, KBr; difference spectrum c, KI. Panel C, spectrum of DMGO contained in 10 mM potassium phosphate buffer, pH 7.5, in the absence (spectrum a) and presence (spectrum b) of 200 mM $NH_4 + CH_3COO^-$. Panel D, difference spectrum of DMGO (spectrum in the presence of salt minus spectrum in the absence of salt) for different ammonium salts. Difference spectrum a, ammonium acetate (200 mM); difference spectrum b, ammonium bicarbonate (200 mM); difference spectrum c, ammonium sulfate (200 mM).

high-resolution gel filtration chromatography, which is approximately twice the subunit molecular mass [89 984 Da; (*29*)]. On the basis of the flavin extinction coefficient (12 700 M^{-1} cm^{-1}), which suggests a single flavin per subunit, we infer the presence of two αN^1-histidyl-FAD moieties per enzyme homodimer.

Salt Effects on the Absorption Properties of DMGO. Purified DMGO in low ionic strength buffer (10 mM potassium phosphate, pH 7.5) exhibits absorption maxima at 352 and 444 nm and a shoulder centered around 464 nm (Figure 2A). The shoulder at 464 nm disappears, and new absorption maxima at 346 and 434 nm are observed on increasing the ionic strength by the addition of NaCl, NH_4-Cl, or KCl (each at 200 mM; Figure 2B). The extent of spectral change is independent of the cation in the chloride salts. The spectral change observed with chloride salts is less pronounced with larger halides (i.e., bromide and iodide; Figure 2B). Addition of ammonium acetate (200 mM) to DMGO also induces a change in the spectral properties. In this case, the shoulder at 464 nm becomes more pronounced compared with DMGO contained in 10 mM potassium phosphate buffer, pH 7.5, alone (Figure 2C). The spectral change is less pronounced on substituting acetate with sulfate and bicarbonate in the ammonium salt (Figure 2D). These spectral analyses indicate perturbation of the electronic absorption spectrum of the flavin in DMGO in the presence and absence of different salts. The observed difference spectra (Figure 2B,D) are similar to those observed with *p*-hydroxybenzoate hydroxylase (PHBH) in complex with different substrates (*40*). In PHBH, the flavin can exist in at least two conformational states: an "in" conformation (observed in the enzyme−*p*-OHB complex), where the flavin is buried within the active site of the protein, and an "out" conformation [observed in the wild-type enzyme complexed with an alternative substrate and in a mutant (Y222F)−*p*-OHB complex], where the isoalloxazine ring is more exposed to solvent (*40*). The effect of various salts on the electronic absorption spectrum of the covalent FAD in DMGO is to alter the properties of the local environment of the isoalloxazine ring. Whether this represents (i) small local conformational differences around the FAD isoalloxazine that affect the degree of solvent exposure, (ii) larger conformational change akin to that seen in PHBH, and/or (iii) binding of the salt anion close to the flavin isoalloxazine ring remains uncertain. We are currently addressing this issue by X-ray analysis of crystals grown under different solution conditions.

Additional evidence for altered states of DMGO was obtained from circular dichroism measurements (Figure 3A,B). The far-UV spectra of DMGO in the presence and absence of NaCl are similar and have a large negative band from 200 to 250 nm with minima at 209 and 220 nm (Figure 3A). Since this region of the spectrum is dominated by transitions of the polypeptide backbone, the data indicate the absence of large changes in protein secondary structure upon addition of NaCl. Small differences in molecular ellipticity were observed in the near-UV region (Figure 3B). The spectra in the presence and absence of NaCl have negative values of ellipticity between 260 and 350 nm; however, the

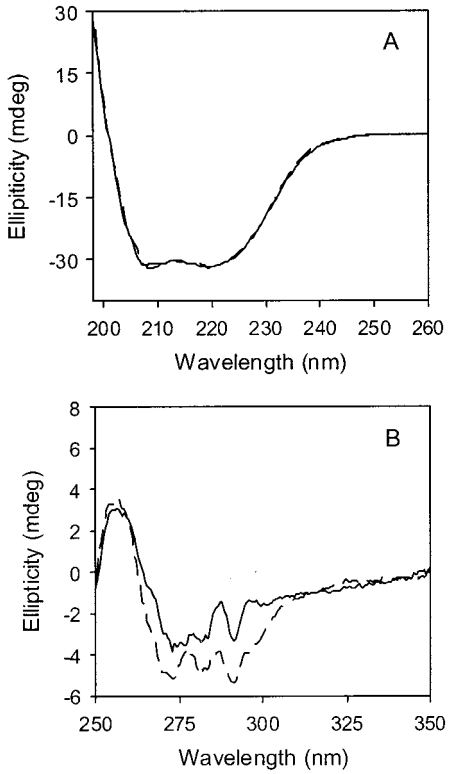

FIGURE 3: Far- and near-UV circular dichroism spectra for DMGO in the presence and absence of NaCl. Panel A, far-UV spectra obtained in the absence and presence (100 mM) of NaCl. Panel B, near-UV spectra; solid spectrum, in the absence of NaCl; dashed spectrum, in the presence of NaCl (100 mM).

intensity of the signal in this region (specifically from 265 to 310 nm) is decreased in the presence of NaCl. Both spectra have a positive peak centered around 256 nm. This region is dominated by contributions from aromatic amino acid residues some of which might form part of, or lie close to, the flavin binding site in DMGO.

Titration of DMGO with Dithionite, Sulfite, and Dimethylglycine. Anaerobic reductive titrations with sodium dithionite indicated that DMGO accepts a maximum of two electrons. Addition of the first electron gives rise to a spectrum that is diagnostic of a red flavin anionic semiquinone (Figure 4A); further reduction gives rise to the spectrum for the hydroquinone. In the conversion of oxidized to semiquinone DMGO, the signature for the red anionic semiquinone has a maximum absorption at 374 nm, and isosbestic points are observed at 349 and 409 nm. On reduction to the hydroquinone, a single isosbestic point was observed at 341 nm. The titration indicates that the redox potentials of the $FAD_{ox.sq}$ and $FAD_{sq.hq}$ couples are sufficiently separated to allow substantial population of the semiquinone species under equilibrium conditions.

DMGO is a typical flavoprotein oxidase as indicated by its reactivity with sodium sulfite (Figure 4B). The dissociation constant (1.6 ± 0.13 mM) for the sulfite−protein complex was calculated from the absorption changes at 444 nm following addition of sulfite (Figure 4B, inset). The titration indicates that both flavins in DMGO behave independently. Reduction of the flavin with the substrate dimethylglycine proceeds directly and stoichiometrically to the two-electron level (hydroquinone) under anaerobic conditions (Figure 4C, and inset). Reduction was also observed with sarcosine, thus establishing that the enzyme does not have absolute specificity for tertiary amine substrates. Reduction by sarcosine, however, was exceptionally slow; the spectral changes shown in Figure 4D are not equilibrium spectra, but show a slow time course (over about 1 h) for DMGO reduction following addition of sarcosine (20 mM).

Stopped-Flow Studies of Flavin Reduction by Dimethylglycine. The reductive half-reaction of DMGO was initially studied at 25 °C under pseudo-first-order conditions using photodiode array detection (Figure 5). Analyses were performed at pH values of 7.5, 8.5, and 9.5 for protiated dimethylglycine and at pH 8.5 for deuterated dimethylglycine. The time-dependent spectra were fitted globally by numerical integration methods using Prokin software (Applied Photophysics). Data collected over a period of 2 s from the mixing event were best fitted to a three-step model (A → B → C → D). Model validity was assessed using the following criteria: the lack of systematic deviations of the residual plot; inspection of the calculated spectra to ensure they make chemical sense in terms of shape and sign; confirmation that the number of significant singular values following singular value decomposition is consistent with the fitted model.

For protiated dimethylglycine, the conversion of each of the enzyme species occurs with similar rates at pH values 7.5, 8.5, and 9.5 (Figure 5). Species A has absorption characteristics of oxidized flavin, and clearly represents the oxidized enzyme (probably as the substrate Michaelis complex). The calculated spectrum for species A is different from that of free enzyme in low ionic strength buffer, and more similar to free enzyme in the presence of 200 mM KCl (Figure 2A). The first kinetic spectrum (Figure 5A,C) suggests, therefore, that the electronic properties of the flavin have been modified following the rapid binding of substrate in the dead time of the stopped-flow instrument. Species B has unusual spectral properties in that there is a broad absorption band from about 350 to 500 nm; the bleaching of flavin absorption suggests the flavin is reduced. However, the spectrum is not that expected for a dihydroflavin. That C−H bond cleavage has occurred on conversion of species A to species B is apparent from the size of the KIE (k^H/k^D = 3.9, for the substrate concentration used in this experiment; and see below for value calculated on the basis of limiting rates of flavin reduction) obtained from comparable studies at pH 8.5 with deuterated dimethylglycine (Figure 5C). The spectral properties of species B are similar (albeit at shorter wavelength) to those reported for the dihydroflavin−imino acid product complexes seen with DAAO (*33*−*35*), and we suggest a similar intermediate forms in the reaction of DMGO. A similar spectral intermediate has also been observed in recent studies with amadoriase I from *Aspergillus* sp. (*41*). In the conversion of species B to C, the characteristic dihydroquinone spectrum is developed. A small spectral change occurs in the conversion of species C to species D, the origin of which is uncertain. However, the flavin clearly remains in the dihydroquinone form. This small spectral change is likely attributable to product release from the enzyme, but its rate of formation is not catalytically important in steady-state reactions (see below). Enzyme oxidation is therefore likely to proceed from species C following collapse of the enzyme−iminium charge-transfer complex.

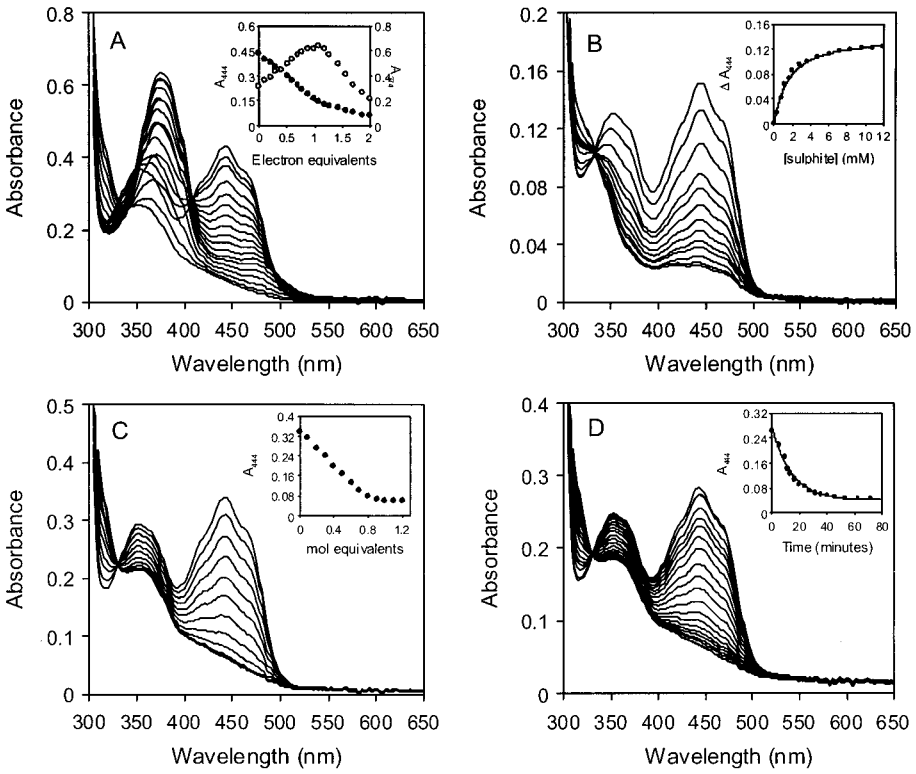

FIGURE 4: Spectral changes for the reductive titration of DMGO with dithionite, sulfite, dimethylglycine, and sarcosine. Panel A, anaerobic reductive titration with sodium dithionite. Inset, plot of absorbance at 444 and 374 nm against electron equivalents. Panel B, sulfite titration of DMGO. Inset, plot of absorbance at 444 nm against sulfite concentration. Data are fitted to a single binding isotherm ($K_d = 1.6 \pm 0.13$ mM). Panel C, reductive titration of DMGO with dimethylglycine. Inset, plot of absorbance at 444 nm versus mole equivalents of dimethylglycine. Panel D, kinetic reduction spectra for reaction of DMGO with sarcosine (20 mM). Conditions: 10 mM potassium phosphate buffer, pH 7.5; 25 °C.

On the basis of the spectral changes observed in the reductive half-reaction, and the KIE observed for the fast phase of the reaction sequence, we propose the following minimal kinetic scheme:

$$EF_{ox} + DMG \underset{k_{-1}}{\overset{k_1}{\rightleftharpoons}} EF_{ox}DMG \underset{k_{-2}}{\overset{k_2}{\rightleftharpoons}} EF_{red}IA \underset{k_{-3}}{\overset{k_3}{\rightleftharpoons}} EF_{red}P \underset{k_{-4}}{\overset{k_4}{\rightleftharpoons}} EF_{red} + P \quad (2)$$

where EF_{ox}, $EF_{ox}DMG$, $EF_{red}IA$, $EF_{red}P$, and EF_{red} are oxidized enzyme, Michaelis complex, the transient reduced enzyme species bound to the putative iminium intermediate, the reduced enzyme bound to the products of iminium hydrolysis, and two-electron-reduced enzyme, respectively. The scheme is similar to that proposed previously for the reaction of DAAO with D-alanine (*34*, *42*) and for the reaction of amadoriase I (*41*).

Single-wavelength stopped-flow studies were performed at 444 nm to investigate the substrate dependence of the individual phases seen in the diode array experiments and to obtain further evidence for the proposed kinetic scheme. Reactions were initially performed in buffer of low ionic strength (10 mM sodium pyrophosphate, pH 8.5), but later extended to higher ionic strength (10 mM sodium pyrophosphate, pH 8.5, 100 mM KCl) to study the potential effects of conformational change on the kinetics of the reductive half-reaction. Transients at 444 nm were triphasic (Figure 6A), consistent with the photodiode array data described above. Conversion of species A → B is dependent on substrate concentration (limiting value of $k_{obs} = k_2 = 244 \pm 6$ s^{-1} as analyzed using eq 4). The limiting value of the rate constant for the fast phase with deuterated substrate is 84 ± 16 s^{-1}. The rates for the intermediate (~16 s^{-1}; species B → C) and slow (~2 s^{-1}; species C → D) phases were found to be independent of substrate concentration (Figure 6C) and not altered by increasing the ionic strength by the addition of KCl (100 mM). The limiting value for conversion of A → B is also unaffected at higher ionic strength, but the limiting value is approached at relatively higher substrate concentration [i.e., ~4-fold increase (from 11 to 42 mM) in the concentration of substrate required to achieve a rate half that of the limiting value for flavin reduction]. These data suggest competitive binding of chloride to the substrate binding site in DMGO.

The observed rate of formation of the E_{red}−IA complex (species B in the diode array experiment) is given by the following equation (*43*):

$$k_{obs} = \frac{k_1[DMG](k_2 + k_{-2}) + k_{-1}k_{-2}}{k_1[DMG] + k_2 + k_{-2} + k_{-1}} \quad (3)$$

Adopting the notation of Porter et al. (*43*), we define $a = k_1(k_2 + k_{-2})$, $b = k_{-1}k_{-2}$, $c = k_1$, and $d = k_2 + k_{-2} + k_{-1}$, and the linear transformation of eq 3 becomes

$$\frac{1}{k_{obs} - b/d} = \frac{cd}{ad - bc} + \frac{d^2}{(ad - bc)[DMG]} \quad (4)$$

The double-reciprocal plot of k_{obs} for formation of the E_{red}−IA complex versus DMG concentration is linear (Figure 6B),

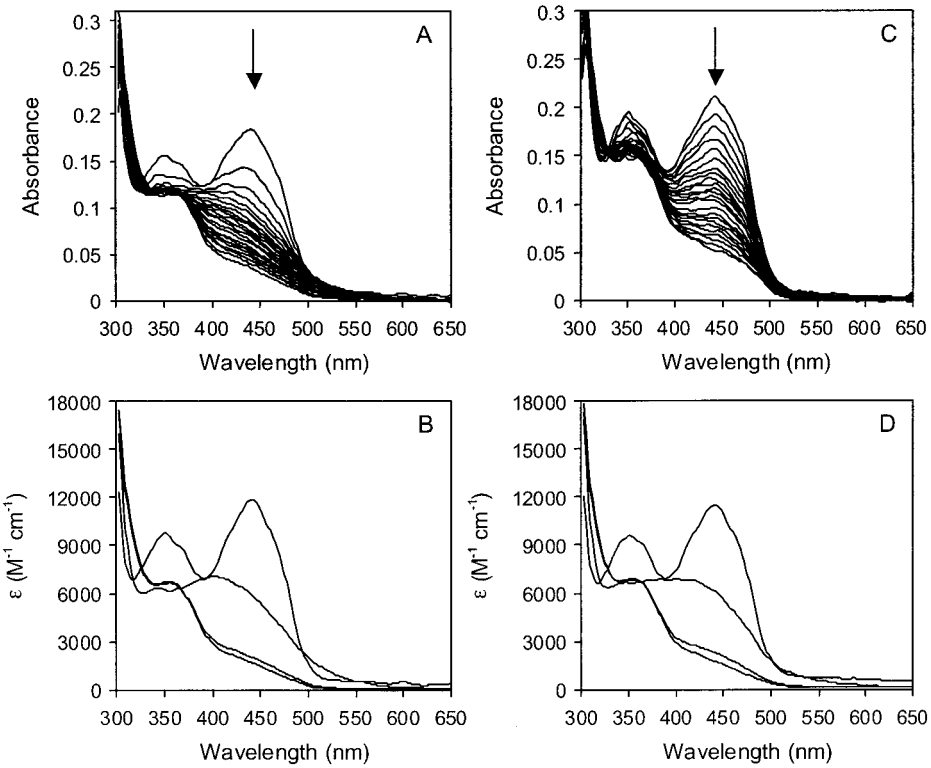

FIGURE 5: Reaction of DMGO with substrate monitored by stopped-flow diode array spectroscopy. Conditions: 10 mM sodium pyrophosphate buffer, pH 8.5; 25 °C. Enzyme concentration, 20 μM; substrate concentration, 30 mM. Panel A, time-dependent spectral changes on mixing DMGO with protiated dimethylglycine at pH 8.5. The experiment is performed over 2 s; the first spectrum is recorded at 1.28 ms. For clarity, only selected spectra are shown. Panel B, deconvoluted spectra for the reaction shown in panel A. The data were fitted to a three-step model. The rate constants obtained from global fitting are 143 ± 3, 15 ± 0.2, and 3.3 ± 0.2 for steps A → B → C → D, respectively. Rate constants obtained at pH 7.5 are 141 ± 3, 14.9 ± 0.2, and 3.7 ± 0.1; rate constants at pH 9.5 are 170 ± 8, 15.6 ± 0.3, and 2 ± 0.07. Panel C, as for panel A, but with deuterated dimethylglycine. Panel D, deconvoluted spectra for data shown in panel C. Rate constants, 36.8 ± 0.9, 14 ± 0.2, and 3 ± 0.1.

indicating that the value of b/d [the apparent first-order rate constant, k_{rev}, for reversal of the reductive half-reaction (*43*)] is much less (i.e., <0.1 s^{-1}, estimated by performing simulations to assess the values of b/d that lead to deviations from linearity) than the value of k_{obs}. In reactions performed with deuterated DMG, the double-reciprocal plot is linear, but importantly not parallel to that observed with protiated DMG (Figure 6B), which contrasts with observations made with DAAO (*43*). For parallel plots, $d^2/(ad - bc)$ is independent of deuterium substitution and hence k_2, and this condition is met when $k_2 + k_{-2} \gg k_{-1}$ and $k_2 \gg k_{-2}$. However, this condition is not met with DMGO. With DMGO, $k_2 \gg k_{-2}$, which implies that the inequality $k_2 \gg k_{-1}$ does not apply. This finding suggests a large value for k_{-1}, which is consistent with the relatively high concentrations (>100 mM) of DMG required to approach the limiting rate for flavin reduction in stopped-flow experiments.

Transients for flavin reduction by sarcosine were essentially monophasic (Figure 7A), owing to the small rate constant for conversion of A → B (i.e., steps B → C and C → D are not kinetically resolved). From plots of the concentration dependence of the rate constant for flavin reduction, the limiting rate of flavin reduction, k_{red} (=0.16 ± 0.01 s^{-1}), and the half-saturating substrate concentration (850 ± 100 mM) were determined (Figure 7B).

Oxidative Half-Reaction of DMGO. The oxidative half-reaction of DMGO was investigated under single-turnover conditions using enzyme reduced stoichiometrically with either sodium dithionite or dimethylglycine. By analogy with the kinetic mechanism of DAAO, the kinetic scheme for a complete catalytic cycle of DMGO is shown (Scheme 1). The oxidative half-reaction can be initiated either at $EF_{red}P$ or at E_{red}, depending on the value of $k_6[O_2]/k_4$. In single-mixing experiments with two-electron-reduced DMGO (reduced artificially by titration with dithionite or by titration with substrate), transients at 444 nm which report on enzyme reoxidation were monophasic (Figure 8A) and linearly dependent on oxygen concentration (Figure 8B). The second-order rate constant (k_5 in Scheme 1) for dithionite- and substrate-reduced DMGO is 342 ± 6 and 201 ± 3 mM^{-1} s^{-1}, respectively. The reduction in the second-order rate constant for substrate-reduced enzyme may indicate that the rate of the oxidative half-reaction is affected by the products of dimethylglycine turnover in the active site of DMGO.

Steady-State Reactions of DMGO. Steady-state reactions of DMGO were performed using the enzyme-monitored turnover method (*39*, *45*) and also using a coupled assay employing horseradish peroxidase with protiated and deuterated dimethylglycine (*29*). Traces for the steady-state turnover of DMGO with different concentrations of reducing substrate are shown in Figure 9 (panels A and B). At 444 nm, there is a rapid, partial decrease in the absorption, followed by the steady-state phase and then a final decrease as the fully reduced enzyme is formed owing to depletion of molecular oxygen. The inset to Figure 9A indicates the spectral forms of DMGO at different points in the multiple-turnover analysis. Initially, the enzyme is essentially oxidized (point A on the trace), but following rapid reduction by

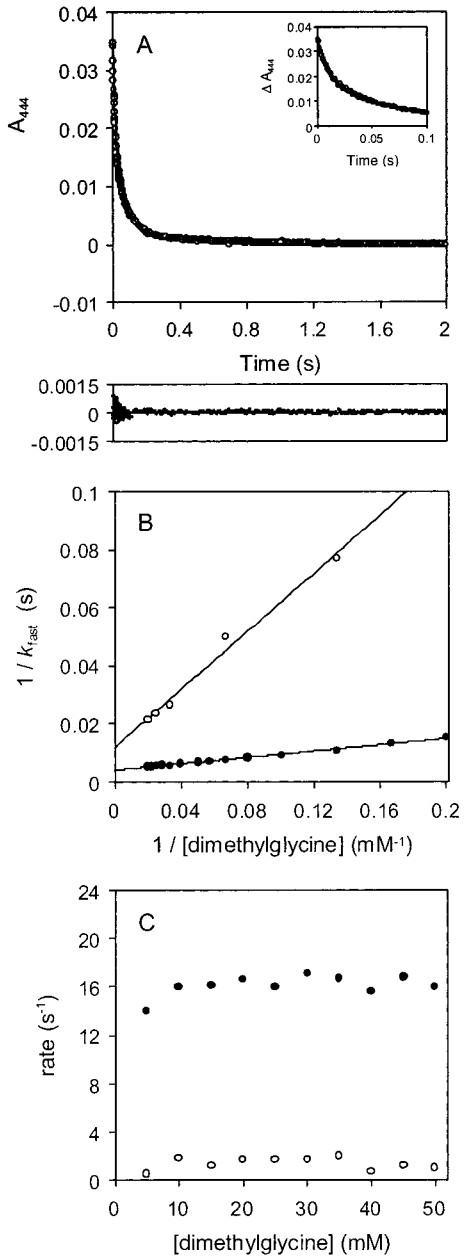

FIGURE 6: Concentration dependence of the kinetics of the reductive half-reaction of DMGO. Conditions: 10 mM sodium pyrophosphate buffer, pH 8.5; 25 °C. Enzyme concentration, 4 μM. Panel A, triphasic absorption transient at 444 nm observed on mixing DMGO with DMG (10 mM); inset, the early time domain of the transient indicating the good fit to a standard triphasic rate expression. Lower panel, plot of residuals from the fit to a triphasic rate expression. Panel B, plot illustrating the concentration dependence of the rate (k_{fast}) of the fast phase observed at 444 nm. Filled circles, protiated substrate (limiting rate 244 $\pm$ 6 s^{-1}); open circles, deuterated substrate (limiting rate 84 $\pm$ 16 s^{-1}). Panel C, concentration dependence of the rate for the intermediate and slow phases of the triphasic transients observed at 444 nm. Filled circles, rates for the intermediate phase; open circles, rates for the slow phase.

substrate and establishment of the steady-state phase (point B on the trace), the spectrum indicates that the enzyme−iminium charge-transfer complex is the predominant species. Following depletion of oxygen (point C on the trace), the enzyme is in the dihydroquinone form. Figure 9B illustrates the traces obtained at different concentrations of reducing substrate. The analysis of these traces was performed as described by Gibson et al. (*39*). The traces represent a record

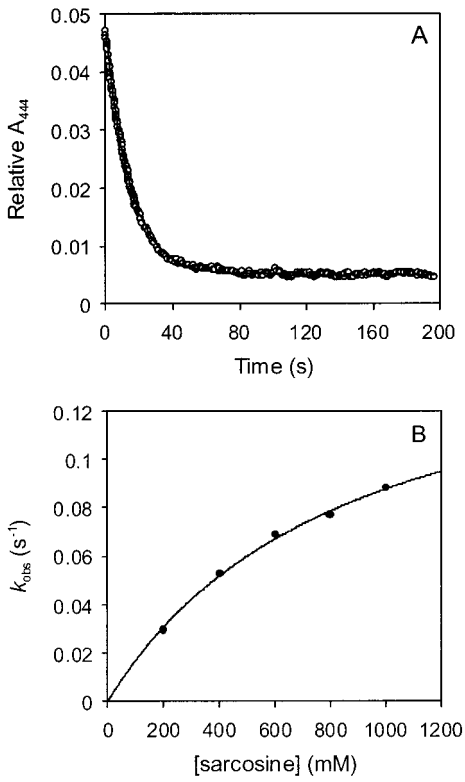

FIGURE 7: Kinetic transient and concentration dependence of the kinetics of the reductive half-reaction of DMGO with sarcosine as substrate. Conditions: 10 mM sodium pyrophosphate buffer, pH 8.5; 25 °C. Enzyme concentration, 4 μM. Panel A, monophasic absorption transient at 444 nm observed on mixing DMGO with sarcosine (600 mM); k_{obs} = 0.069 s^{-1}. Panel B, plot illustrating the concentration dependence of the rate (k_{obs}) of flavin bleaching observed at 444 nm. Limiting rate 0.16 $\pm$ 0.01 s^{-1}; half-saturating concentration, 850 $\pm$ 100 mM.

Scheme 1

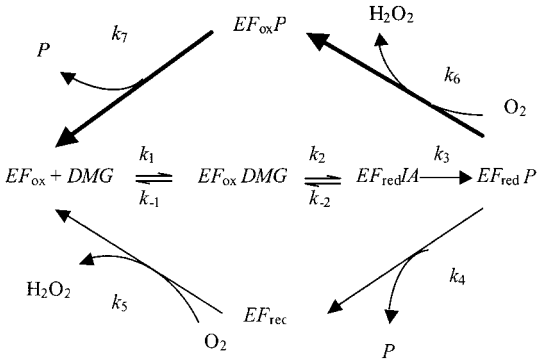

of the rate of catalysis as a continuous function of oxygen concentration. Figure 10A indicates that a series of parallel lines are obtained on plotting the reciprocal of the turnover number versus the reciprocal of the oxygen concentration. A secondary plot of the ordinate intercept versus dimethylglycine concentration is shown in Figure 10B. The ordinate intercept of this secondary plot (10.6 $\pm$ 0.4 s^{-1}) is the true turnover number, k_{cat}, for the steady-state reaction. The true K_m for dimethylglycine (2.4 $\pm$ 0.2 mM) is derived from this plot by dividing the value of the gradient by the ordinate intercept. The true K_m for molecular oxygen (0.041 $\pm$ 0.003 mM) was obtained by taking the slope of any line in Figure 10A (in this case the 5 mM dimethylglycine line) divided by the intercept of the line in Figure 10B.

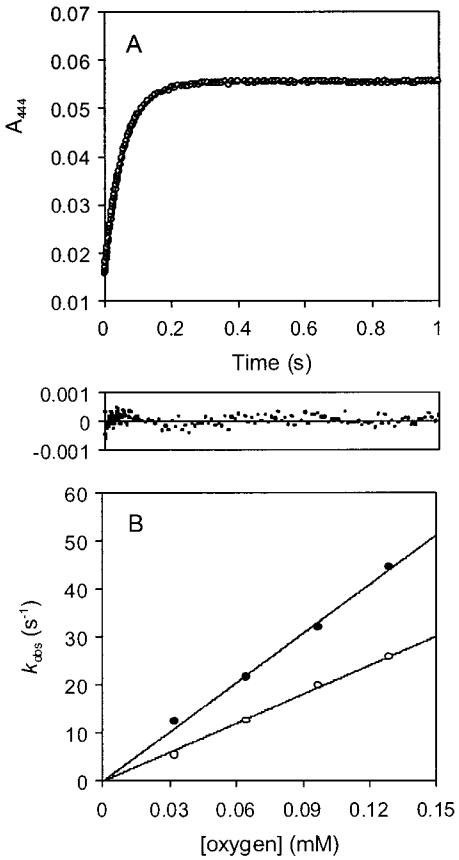

FIGURE 8: Kinetics of the oxidative half-reaction of DMGO. Conditions: 10 mM sodium pyrophosphate buffer, pH 8.5; 25 °C. Enzyme concentration, 5 μM. Panel A, monophasic kinetic transient observed for the oxidation of dithionite-reduced DMGO by molecular oxygen (0.065 mM). Lower panel, plot of residuals for data fitting to a monophasic rate expression. Panel B, plot of observed rate of flavin oxidation versus oxygen concentration for dithionite-reduced (filled circles) and substrate-reduced (open circles) DMGO. Bimolecular rate constants are 342 mM s^{-1} (dithionite-reduced enzyme) and 201 mM s^{-1} (substrate-reduced enzyme).

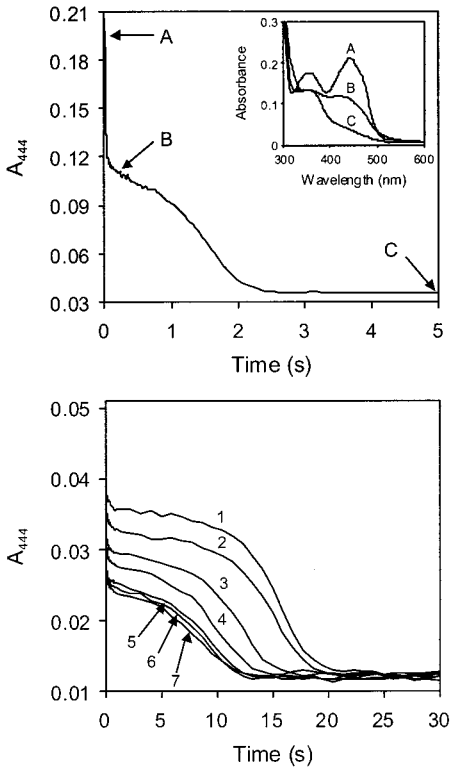

FIGURE 9: Enzyme-monitored turnover of DMGO in the stopped-flow instrument. Upper panel, enzyme (4 μM) reacted with 10 mM DMG in 10 mM sodium pyrophosphate buffer, pH 8.5; 25 °C. The course of reaction was monitored at 444 nm versus time. Arrow A shows the initial absorption, which is initially rapidly bleached as a result of flavin reduction, prior to establishing steady-state conditions. Inset, spectrum of the enzyme recorded with a photodiode array detector at the indicated selected points in the time course of the main panel; oxygen concentration was 0.258 mM. Lower panel, as for upper panel, but with different concentrations of the reducing substrate. Curves 1 to 7 are for DMG concentrations of 1, 2, 5, 10, 20, 30, and 40 mM, respectively.

Owing to limited supplies of deuterated dimethylglycine, the steady-state behavior of DMGO was also investigated using the more conventional coupled assay employing horseradish peroxidase. Apparent Michaelis constants for protiated and deuterated dimethylglycine are 3.4 ± 0.2 and 13.3 ± 1.4 mM, respectively. The apparent turnover number, k_{cat}, with protiated and deuterated substrate is 9.6 ± 0.2 and 6.9 ± 0.3 s^{-1}, respectively. The kinetic parameters for protiated substrate are comparable with those measured using the enzyme-monitored turnover method.

DISCUSSION

Our stopped-flow studies have established that the kinetic mechanism of substrate oxidation by DMGO is similar to that of DAAO (*33*−*35*, *43*) and other oxidases (*36*, *37*, *41*) that form a labile iminium−enzyme charge-transfer intermediate. The spectral properties of DMGO in stopped-flow reactions with reducing substrate indicate the presence of four enzyme species (A−D). Species D is not catalytically important since its rate of formation (2 s^{-1}) is less than the steady-state turnover number (10.6 s^{-1}), and is attributed to two-electron-reduced enzyme (i.e., in the absence of bound products). The spectral properties on conversion of species A to C seen in our photodiode array experiments are similar to those observed in kinetic studies with DAAO (*43*), suggesting the formation of a reduced enzyme−iminium charge-transfer intermediate (species B). Deprotonation and hydrolysis of the iminium charge-transfer intermediate yield species C, which we suggest represents two-electron-reduced enzyme bound to the products of iminium hydrolysis. The overall catalytic cycle is shown in Scheme 1, with the reductive half-reaction depicted as the central route from EF_{ox} to $EF_{red}P$. In Scheme 1, k_4 represents conversion of species C to species D, which imposes a kinetic bottleneck and thus prevents passage through the lower loop for enzyme oxidation during steady-state turnover. Oxidation of enzyme during steady-state turnover therefore proceeds from $EF_{red}P$ through the upper loop of Scheme 1, and our enzyme-monitored turnover studies indicate that decay of $EF_{red}IA$ (16 s^{-1}) is the main contributing step to rate limitation in steady-state turnover (k_{cat} = 10.6 s^{-1}). The microscopic rate constants for those reaction steps of Scheme 1 that have been measured in our kinetic studies are given in Table 1.

The kinetics of the upper loop in Scheme 1 cannot be measured by standard stopped-flow, single-mixing methods because $EF_{red}P$ and $EF_{ox}P$ are transient intermediates and cannot be used to initiate the reaction. In principle, the sequential mixing technique could be used to measure the rate constants for enzyme oxidation from the $EF_{red}P$ intermediate by dioxygen and product release from oxidized enzyme. The method would involve either (i) reduction of enzyme with stoichiometric substrate to generate transiently

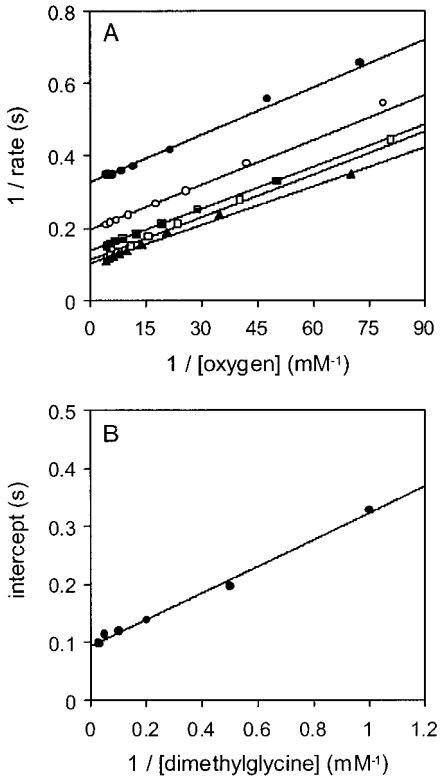

FIGURE 10: Panel A, double-reciprocal plots of the data shown in Figure 9B, obtained as described by Gibson et al. (*39*). Symbols: filled circles, 1 mM DMG; open circles, 2 mM DMG; filled squares, 5 mM DMG; open squares, 20 mM DMG; filled triangles, 30 mM DMG. For clarity, only selected lines on the reciprocal plot corresponding to the range of DMG concentrations shown in Figure 9B are shown. Panel B, a secondary plot of the ordinate intercepts of lines from the reciprocal plot (Figure 10A) as a function of DMG concentration.

Table 1: Steady-State and Microscopic Rate Constants for DMGO at pH 8.5 and 25 °C[a]

parameter	value	parameter	value
k_{cat}	10.6 s^{-1}	k_3	16 s^{-1}
K_m^{DMG}	2.4 mM	k_4	2 s^{-1}
$K_m^{O_2}$	0.041 mM	k_5	342 mM^{-1} s^{-1}
k_2	224 s^{-1}	k_7[b]	36 s^{-1}

[a] Steady-state parameters are those from enzyme-monitored turnover experiments. [b] Calculated using eq 5 and setting $k_{-2} = 0$.

the labile intermediate prior to the second mix containing aerobic buffer, or (ii) reduction of the enzyme with excess substrate to generate the labile intermediate prior to the second mix containing aerobic buffer and a competitive inhibitor which prevents multiple turnover. The latter method was used successfully with DAAO (*43*), and we have used the first method in studies of the oxidative half-reaction of bacterial morphinone reductase (*44*). Neither method, however, is appropriate with DMGO; a suitable competitive inhibitor of the enzyme is not available, and stoichiometric reduction by DMG is too slow to enable accumulation of the $EF_{red}P$ intermediate. It is, therefore, not possible to determine the value of k_6 in a stopped-flow experiment. We have, however, performed multiple-turnover studies of DMGO using photodiode array detection. These studies indicate that the $EF_{red}IA$ intermediate accumulates under steady-state conditions (Figure 9 and inset). Since this intermediate decays in single-turnover studies with a rate $\sim$16 s^{-1}, we can confidently state that enzyme oxidation from the $EF_{red}P$ intermediate occurs at a rate significantly greater than 16 s^{-1}.

It was not possible to measure k_6 owing to difficulties in generating the labile $EF_{red}P$ intermediate for stopped-flow studies. An approximate value for k_7 was calculated from eq 5, and our studies of the oxidative half-reaction have allowed us to measure directly the value of k_5. The small difference in the value of k_5 measured in experiments performed with dithionite-reduced and substrate-reduced enzyme may indicate a mixed population of EF_{red} and $EF_{red}P$ at the start of the stopped-flow experiment with substrate-reduced enzyme. For this reason, the rate constant measured with dithionite-reduced enzyme is likely to be more representative of the true value of k_5. Our kinetic studies have not allowed us to measure k_1 and k_{-1}, although we assume rapid, bimolecular association of enzyme with substrate. An upper value for this association (i.e., approximately 10^6 M^{-1} s^{-1}) would set k_{-1} at about 10^4 s^{-1}. This latter value is determined from approximate fitting of stopped-flow data using the rapid equilibrium formalism of Strickland et al. (*46*), which indicates a K_d value of 10 mM for formation of the enzyme−substrate complex $EF_{ox}DMG$. The lack of an obvious intercept on fitting stopped-flow data to the Strickland equation indicates that formation of $EF_{red}IA$ is essentially irreversible (i.e., k_{-2} is close to zero). Given that k_{-1} is likely to be relatively large (approximately 10^4 s^{-1}), the small value of k_{-2} is also apparent from the linear double-reciprocal plot shown in Figure 6B (as the value of k_{-2} increases, the plot deviates from linearity).

The isotope effect on k_{cat} ($^Hk_{cat}/^Dk_{cat} = 1.4 \pm 0.1$) is small, but suggests some contribution to rate limitation from the bond cleavage step. This can be rationalized from the following expression for k_{cat}, which can be derived for Scheme 1 (*41*):

$$k_{cat} = \left[\frac{k_{-2} + k_3}{k_2 k_3} + \frac{1}{k_3} + \frac{1}{k_7}\right]^{-1} \quad (5)$$

From our stopped-flow studies, we have calculated values for k_2 and k_3 (244 and 16 s^{-1}, respectively). The value for k_{-2} is likely to be comparatively small ($\ll$10 s^{-1}), since there is no obvious intercept in the plot of k_{obs} versus DMG concentration for flavin reduction when analyzed approximately using the rapid equilibrium formalism of Strickland et al. (*46*). To obtain a true k_{cat} value of 10.6 s^{-1} for protiated DMG, a value of 36 s^{-1} for k_7 (which we have been unable to measure directly) is required. This suggests that decay of the reduced enzyme−iminium charge-transfer complex is the main contributing factor to rate limitation in the steady-state, which is entirely consistent with the results of our enzyme-monitored turnover experiment in which the reduced enzyme−iminium complex is the major species under steady-state conditions (Figure 9A, inset).

The overall reaction catalyzed by DMGO is similar to that catalyzed by other flavoprotein amine oxidases such as MSOX and TSOX, the only difference being that the substrate for sarcosine oxidases contains one less methyl group. Oxidation of sarcosine by sarcosine oxidases likely proceeds through the formation of a labile iminium intermediate, as indeed do reactions catalyzed by other flavoprotein oxidases/dehydrogenases such as that catalyzed by trimethylamine dehydrogenase (TMADH). However, stopped-flow kinetic studies with MSOX (*47*) and TSOX (*14*), and with TMADH (*26*), have failed to identify transient enzyme−

iminium charge-transfer complexes in the reductive half-reaction, perhaps indicating the lack of an electronic interaction of the iminium intermediate with the enzyme dihydroflavin. An alternative explanation may be that the rate of hydrolysis of the iminium intermediate is faster than its formation in those enzymes where enzyme−iminium charge-transfer complexes are not observed. We can therefore identify two distinct types of flavoprotein oxidases—those in which a reduced enzyme−iminium charge-transfer intermediate forms as a result of substrate oxidation and those in which the generated iminium is not seen to interact electronically with the enzyme flavin. Clearly, further studies are required to ascertain why the iminium−enzyme charge-transfer complex forms in only some flavoprotein amine oxidases, and this will involve a combination of functional and structural work. The structures of MSOX, TMADH, and DAAO have been reported (*6*, *48*). Our current work is now focused on the structural elucidation of DMGO to enable comparison with MSOX, TMADH, and DAAO.

Conclusions. Our studies have established that DMGO contains an αN^1-histidyl^{48}-FAD and is a typical flavoprotein oxidase, showing reactivity with sulfite. The electronic absorption spectrum of the covalently linked FAD is perturbed by the addition of a number of salts, suggesting different conformational states and/or specific binding sites for small anions close to the flavin isoalloxazine ring. The kinetic mechanism of DMGO is similar to that determined for DAAO and other enzymes that form a labile enzyme−iminium charge-transfer intermediate, and distinct from the kinetic mechanisms of MSOX and TSOX which overall catalyze reactions that are very similar to that of DMGO. Based on the presence or absence of an enzyme−iminium charge-transfer intermediate in the reductive half-reaction, we propose the existence of at least two classes of flavoprotein amine oxidase.

REFERENCES

1. Tabor, C. W., and Tabor, H. (1984) *Annu. Rev. Biochem. 53*, 749−790.
2. Pegg, A. E. (1986) *Biochem. J. 234*, 249−262.
3. Pegg, A. E. (1988) *Cancer Res. 48*, 759−774.
4. Poulin, R., Pelletier, G., and Pegg, A. E. (1995) *Biochem. J. 311*, 723−727.
5. Hu, R. H., and Pegg, A. E. (1997) *Biochem. J. 328*, 307−316.
6. Trickey, P., Wagner, M. A., Jorns, M. S., and Mathews, F. S. (1999) *Structure 7*, 331−345.
7. Trickey, P., Basran, J., Lian, L. Y., Chen, Z., Barton, J. D., Sutcliffe, M. J., Scrutton, N. S., and Mathews, F. S. (2000) *Biochemistry 39*, 7678−7688.
8. Parsons, M. R., Convery, M. A., Wilmot, C. M., Yadav, K. D., Blakeley, V., Corner, A. S., Phillips, S. E., McPherson, M. J., and Knowles, P. F. (1995) *Structure 3*, 1171−1184.
9. Li, R., Klinman, J. P., and Mathews, F. S. (1998) *Structure 6*, 293−307.
10. Chen, L., Durley, R. C., Mathews, F. S., and Davidson, V. L. (1994) *Science 264*, 86−90.
11. Basran, J., Sutcliffe, M. J., and Scrutton, N. S. (2001) *J. Biol. Chem. 276*, 42887−42892.
12. Murray, J. M., Saysell, C. G., Wilmot, C. M., Tambyrajah, W. S., Jaeger, J., Knowles, P. F., Phillips, S. E., and McPherson, M. J. (1999) *Biochemistry 38*, 8217−8227.
13. Wagner, M. A., Trickey, P., Chen, Z. W., Mathews, F. S., and Jorns, M. S. (2000) *Biochemistry 39*, 8813−8824.
14. Harris, R. J., Meskys, R., Sutcliffe, M. J., and Scrutton, N. S. (2000) *Biochemistry 39*, 1189−1198.
15. Davidson, V. L., Jones, L. H., and Graichen, M. E. (1992) *Biochemistry 31*, 3385−3390.
16. Halcrow, M., Phillips, S., and Knowles, P. (2000) in *Enzyme catalyzed electron and radical transfer* (Holzenburg, A., and Scrutton, N. S., Eds.) pp 183−231, Kluwer Academic/Plenum, London and New York.
17. Davidson, V. (2000) in *Enzyme catalysed electron and radical transfer* (Holzenburg, A., and Scrutton, N. S., Eds.) pp 119−143, Kluwer Academic/Plenum, London and New York.
18. Basran, J., Sutcliffe, M. J., and Scrutton, N. S. (1999) *Biochemistry 38*, 3218−3222.
19. Basran, J., Patel, S., Sutcliffe, M. J., and Scrutton, N. S. (2001) *J. Biol. Chem. 276*, 6234−6242.
20. Grant, K. L., and Klinman, J. P. (1989) *Biochemistry 28*, 6597−6605.
21. Jonsson, T., Edmondson, D. E., and Klinman, J. P. (1994) *Biochemistry 33*, 14871−14878.
22. Basran, J., Sutcliffe, M. J., and Scrutton, N. S. (2001) *J. Biol. Chem. 276*, 24581−24587.
23. Kim, J.-M., Bogdon, M. A., and Mariano, P. S. (1993) *J. Am. Chem. Soc. 115*, 10591−10595.
24. Silverman, R. B. (1995) *Acc. Chem. Res. 28*, 335−342.
25. Edmondson, D. E. (1995) *Xenobiotica 25*, 735−753.
26. Jang, M.-H., Basran, J., Scrutton, N. S., and Hille, R. (1999) *J. Biol. Chem. 274*, 13147−13154.
27. Miller, J. R., and Edmondson, D. E. (1999) *Biochemistry 38*, 13670−13683.
28. Miura, R., Setoyama, C., Nishina, Y., Shiga, K., Mizutani, H., Miyahara, I., and Hirotsu, K. (1997) *J. Biochem. (Tokyo) 122*, 825−833.
29. Meskys, R., Harris, R. J., Casaite, V., Basran, J., and Scrutton, N. S. (2001) *Eur. J. Biochem. 268*, 3390−3398.
30. Binzak, B. A., Vockley, J. G., Jenkins, R. B., and Vockley, J. (2000) *Mol. Genet. Metab. 69*, 181−187.
31. Eschenbrenner, M., and Jorns, M. S. (1999) *Genomics 59*, 300−308.
32. Kvalnes-Krick, K., and Jorns, M. S. (1986) *Biochemistry 25*, 6061−6069.
33. Kubo, H., Watari, H., and Shiga, T. (1959) *Bull. Soc. Chim. Biol. 41*, 981−988.
34. Massey, V., and Gibson, Q. H. (1964) *Fed. Proc., Fed. Am. Soc. Exp. Biol. 23*, 18−29.
35. Yagi, K., Okamura, K., Naoi, M., Sugiura, N., and Kotaki, A. (1967) *Biochim. Biophys. Acta 146*, 77−90.
36. Kumagai, H., Yamada, H., Suzuki, H., and Ogura, Y. (1971) *J. Biochem. (Tokyo) 69*, 137−144.
37. Koyama, H., and Suzuki, H. (1986) *J. Biochem. (Tokyo) 100*, 859−866.
38. Leatherbarrow, R. J. (1992) Erithacus Software Ltd, Staines, U.K.
39. Gibson, Q. H., Swoboda, B. E. P., and Massey, V. (1964) *J. Biol. Chem. 239*, 3927−3934.
40. Gatti, D. L., Palfey, B. A., Lah, M. S., Entsch, B., Massey, V., Ballou, D. P., and Ludwig, M. L. (1994) *Science 266*, 110−114.
41. Wu, X., Palfey, B. A., Mossine, V. V., and Monnier, V. M. (2001) *Biochemistry 40*, 12886−12895.
42. Nakamura, T., Nakamura, S., and Ogura, Y. (1963) *J. Biochem. 54*, 512−519.
43. Porter, D. J., Voet, J. G., and Bright, H. J. (1977) *J. Biol. Chem. 252*, 4464−4473.
44. Craig, D. H., Moody, P. C., Bruce, N. C., and Scrutton, N. S. (1998) *Biochemistry 37*, 7598−7607.
45. Chance, B. (1943) *J. Biol. Chem. 151*, 553−577.
46. Strickland, S., Palmer, G., and Massey, V. (1975) *J. Biol. Chem. 250*, 4048−4052.
47. Wagner, M. A., and Jorns, M. S. (2000) *Biochemistry 39*, 8825−8829.
48. Mattevi, A., Vanoni, M. A., Todone, F., Rizzi, M., Teplyakov, A., Coda, A., Bolognesi, M., and Curti, B. (1996) *Proc. Natl. Acad. Sci. U.S.A. 93*, 7496−7501.

BI025519H